Intrinsic Josephson effects in high-T_c superconductors

R. Kleiner and P. Müller
Walther-Meissner-Institut, D-85748 Garching, Germany
(Received 19 July 1993)

We have investigated the coupling between CuO_2 layers in high-T_c superconductors by direct measurements of all dc and ac Josephson effects with current flow in the c-axis direction. The measurements have been performed on small single crystals of $Bi_2Sr_2CaCu_2O_8$, $(Pb_yBi_{1-y})_2Sr_2CaCu_2O_8$, $Tl_2Ba_2Ca_2Cu_3O_{10}$, and $YBa_2Cu_3O_{7-x}$ and on a-axis-oriented $YBa_2Cu_2O_7$ thin films. The results clearly show that all materials behave like stacks of superconductor-insulator-superconductor Josephson junctions. The current-voltage characteristics exhibit large hystereses and multiple branches, which can be explained by a series connection of highly capacitive junctions. From the modulation of the critical current in a magnetic field parallel to the layers, we infer a junction thickness of approximately 15 Å. In our microwave emission experiments we were able to prove explicitly that every pair of CuO_2 double or triple layers forms a working Josephson contact. An exception is $YBa_2Cu_3O_7$, where only flux-flow behavior has been observed.

I. INTRODUCTION

The essential universal characteristic of the superconducting state is the existence of a many-particle condensate wave function, which maintains phase coherence over macroscopic distances. Manifestations of this fact are the Meissner effect, flux quantization, and the Josephson effects.[1] The classic low-temperature superconductors exhibit coherence regions, which extend over several lattice constants. Any point defects or anisotropies of the crystal lattice influence the superconducting state in a rather indirect way. In the high-temperature superconductors, however, the superconducting Ginzburg-Landau coherence lengths are, at least, comparable to the separation of typical structural elements such as the CuO_2 planes. Therefore, regardless of the still-unknown coupling mechanism, it appears worthwhile to ask whether the superconducting order parameter is spatially constant, i.e., whether even perfect high-T_c single crystals are homogeneous superconductors or not.

Anisotropic layered superconductors such as some transition-metal dichalcogenides and their intercalated compounds ($NbSe_2$, TaS_2, $TaSe_2$), the organic superconductors (the Bechgaard salts and the BEDT-TTF family), and artificial multilayers (Nb-Cu, Nb-NbO_x, Pb-Ge, Au-Ge, Pb-Au) have been under research since the early 1970s.[2–27] In all of these structures, superconducting layers alternate with weakly superconducting, normal, or even insulating layers. In some of the compounds, the Ginzburg-Landau coherence length perpendicular to the superconducting layers is comparable or smaller than the interlayer spacing, which indicates that these materials cannot be treated simply as extremely anisotropic but still homogeneous materials. Even in a perfect single crystal, the amplitude of the superconducting order parameter should vary strongly between the layers. This situation, which is well known from Josephson junctions, leads to the idea that, at least for the most anisotropic materials, the superconducting layers are coupled by the Josephson effect. A macroscopic theory for such systems has been proposed by Lawrence and Doniach.[28] The theory was quite successful in explaining the temperature and angular dependence of the upper critical fields.[17,18,26,29] Up to now, however, we do not know of any direct measurements of dc and ac Josephson effects in these materials.

It can be assumed that in the high-T_c superconductors the Cooper pairs are concentrated to the CuO_2 planes. In the most anisotropic materials such as Bi_2Sr_2 $CaCu_2O_8$ (BSCCO), which contains CuO_2 double layers separated by Bi_2O_3 and SrO layers, the critical transport current densities along the CuO_2 planes (the *ab* direction) are at least two orders in magnitude larger than those perpendicular to the layers (the *c* direction). The anisotropy ratio of the magnetic-field penetration depths, $\gamma=\lambda_{ab}/\lambda_c$, can be as large as 1000.[30] The c-axis Ginzburg-Landau coherence lengths ξ_c inferred from H_{c2} measurements are less than 1 Å, i.e., more than 10 times smaller than the spacing between adjacent CuO_2 double layers.[29] Again, such subatomic coherence lengths rule out any mean-field description. Nevertheless, this extremely small value of ξ_c makes BSCCO a good candidate for a Josephson-coupled superconductor. Experiments by Bozovic *et al.*[31] have shown that superconductivity in a 15.5-Å-thick molecular layer containing only one CuO_2 double layer is not degraded by the presence of adjacent nonsuperconducting material. Therefore the simplest approach is to assume that the CuO_2 double layers act as 3-Å-thick superconducting electrodes separated by insulating, semiconducting, or normal layers. From this point of view a 3-μm-thick single crystal consists of a stack of 2000 closely packed interacting Josephson junctions. Measurements of the angular dependence of the critical current,[32] the upper critical field,[33] the torque,[30] or the peculiarities of vortex motion under the influence of a temperature gradient[34,35] support this picture.

In our work we focused on direct measurements of all ac and dc Josephson effects using small BSCCO single crystals.[36–44] The results show clearly that BSCCO

behaves like a stack of superconductor-insulator-supercondcutor Josephson junctions, i.e., that the coupling between adjacent CuO_2 double layers is truly Josephson-like. The aim of this paper is to discuss the results obtained in BSCCO in detail and to present additional results on lead-substituted bismuth compounds $(Pb_yBi_{1-y})_2Sr_2CaCu_2O_8$ (PBSCCO), $Tl_2Ba_2Ca_2Cu_3O_{10}$ (TBCCO), and $YBa_2Cu_3O_7$ (YBCO) single crystals.

The paper is organized as follows: In Sec. II the basic properties of a stack of Josephson junctions and their consequences for the observability of ac and dc Josephson effects in high-T_c single crystals are introduced. Sections III and IV present sample characterization and measuring techniques. Results are discussed in Sec. V, arranged according to the different types of measurement: (i) I-V characteristics, with transport currents in the c-axis direction, (ii) temperature dependence of the c-axis critical current I_c, (iii) magnetic-field dependence of I_c, (iv) microwave absorption, and (v) microwave emission. Finally, in Sec. VI, the three systems BSCCO, TBCCO, and YBCO are compared.

II. BASIC CONCEPTS

The following section contains a discussion of the basic properties of a stack of Josephson junctions. As discussed above, this is the simplest model for a Josephson-coupled layered structure. Therefore we will assume that BSCCO actually is a stack of coupled Josephson junctions. We then have to work out the characteristic features of this model and perform the necessary experiments—the ac and dc Josephson effects—to prove or disprove it.

The geometry of our model can be described as follows (Fig. 1).

(i) The CuO_2 double layers and the enclosed Ca layer form superconducting electrodes of thickness $d=3$ Å.

(ii) The Bi_2O_3 and SrO layers act as an insulating, semiconducting, or normal barrier of thickness $t=12$ Å. For the sake of simplicity, we will not distinguish between the electronic properties of the Bi_2O_3 and SrO layers; i.e., we will characterize the elementary Josephson junctions as either SIS (superconductor-insulator-superconductor) or SNS (superconductor-normal-metal-superconductor) junctions. We will not discuss more complicated structures such as SINIS or SNINS junctions.

(i) A single Josephson junction within the stack therefore has a thickness of 15 Å. A single crystal of 3 μm thickness will be regarded as a stack of $N=2000$ of such junctions.

(ii) The supercurrents in the c direction across the nth Josephson junction within the stack, j_{zn}, will be described by the two Josephson equations

$$j_{zn}=j_c\sin(\gamma_n)\ , \tag{1}$$

$$\hbar\dot{\gamma}_n=2eV_n\ , \tag{2}$$

where γ_n is the (gauge-invariant) phase difference of the order parameter in the electrodes of the nth junction and V_n is the voltage across the nth junction.

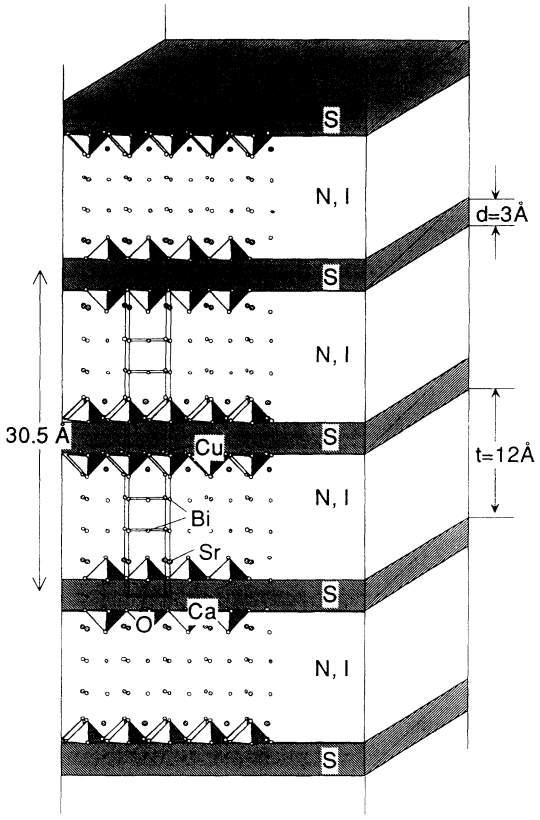

FIG. 1. Superposition of the BSCCO crystal structure and a stack of Josephson junctions, whose electrodes are formed by CuO_2 double layers.

Some simple estimates for characteristic junction parameters in terms of the resistively shunted junction (RSJ) model[45] can be made from the above geometry:

Characteristic voltage $V_c=I_cR$. For a SIS junction, the Ambegaokar-Baratoff relation[46]

$$I_cR_n=\frac{\pi}{2e}\Delta\tanh\left[\frac{\Delta}{2k_BT}\right] \tag{3}$$

holds. R_n is the junction's normal resistance, and Δ is the energy gap. This value of I_cR_n can be regarded as an upper limit for the characteristic voltage. Taking $\Delta=11$ meV according to the BCS ratio formula (3) yields $V_c=18$ mV at $T=0$. Of course, V_c can be drastically reduced as a result of localized states[47,48] or parasitic shunt resistances.

Characteristic frequency f_c. The characteristic frequency is defined as $f_c=V_c/\Phi_0$ (Φ_0 is the flux quantum). Using $V_c=18$ mV yields $f_c\approx 9$ THz.

Plasma frequency $f_{\rm pl}$. The plasma frequency is given by

$$f_{\rm pl}=\left[\frac{I_c}{2\pi\Phi_0C}\right]^{1/2}=\left[\frac{j_ct}{2\pi\Phi_0\epsilon\epsilon_0}\right]^{1/2}\ , \tag{4}$$

where C is the junction capacitance, ϵ is the dielectric constant and t is the barrier thickness. We have found

critical current densities in the c direction ranging from 100 up to 7000 A/cm^2 (cf. Sec. III). Assuming $\epsilon=10$ yields plasma frequencies between 10 and 100 GHz.

McCumber parameter β_c. The shape of the *I-V* characteristic is essentially determined by the McCumber parameter $\beta_c=(f_c/f_{\rm pl})^2$. For $\beta_c>1$ the *I-V* characteristics are hysteretic, the return current decreasing with increasing β_c. Using the above estimates of f_c and $f_{\rm pl}$ yields very large values of β_c. Therefore we expect highly hysteretic *I-V* characteristics, at least in the case of an insulating barrier.

Important consequences can be drawn from the fact that the thickness of the electrodes is only 3 Å in our model system: Whereas the electrodes in usual Josephson junctions are much thicker than the London penetration depth, in our case the ratio d/λ_{ab} only is 0.001 ($\lambda_{ab}\approx 1700$ Å,[49] where the subscript denotes the direction of the screening current flow). In this case those currents flowing in the ab direction will couple adjacent Josephson junctions, which share one electrode. Also, the large kinetic inductance of these currents will influence the gradient of the phase difference γ along the a and b directions. Whereas the properties of large Josephson junctions with thick ($d\gg\lambda$) electrodes have been studied extensively,[50] only a few authors have investigated the opposite limit.[51–53] We therefore will derive the basic equations describing the local variations of the phase gradient γ in the static case in order to quantify the effect of the thin electrodes and to introduce the relevant length scales. A stack of N Josephson junctions is shown in Fig. 2(a). The length of the stack in the x direction is b; its width in the y direction is a. Here a is assumed to be small compared to the characteristic lengths λ_c and λ_j introduced later. An external magnetic field H is applied along y; the bias current $j_{\rm ext}$ is fed into the outermost electrodes labeled 0 and N. The phase of the order parameter is φ_n and

$$\gamma_n=\varphi_n-\varphi_{n-1}-2e/\hbar\int_{(n-1)(t+d)}^{n(t+d)}A_z dz\ ,\qquad n=1,\ldots,N\ .$$

If variations of the amplitude of the order parameter inside the electrodes can be neglected, the gradient of φ_n is given by

$$\nabla\varphi_n=\frac{2e}{\hbar}(\mathbf{A}+\mu_0\lambda_{ab}^2\mathbf{j}_{x,n})\ . \tag{5}$$

$\mathbf{j}_{x,n}$ denotes the supercurrents flowing along the nth electrode, and $\mathbf{A}$ is the vector potential.

Integrating (5) along the line shown in Fig. 2(a) yields

$$\gamma_n'=\frac{d\gamma_n}{dx}=\frac{2\pi\mu_0(t+d)H_{y,n}}{\Phi_0}+\frac{2\pi}{\Phi_0}\mu_0\lambda_{ab}^2(j_{x,n}-j_{x,n-1})\ . \tag{6}$$

Whereas the contribution of the currents $j_{x,n}$ is (exponentially) small in the thick electrode limit, it plays a dominant role here.

The currents $j_{x,n}$ can be related to the c-axis currents using the continuity equations [Fig. 2(b)]

$$\begin{aligned}j_n'&=\frac{1}{d}[j_c\sin(\gamma_n)-j_c\sin(\gamma_{n+1})],\quad n=1,\ldots,N-1\ ,\\ j_0'&=\frac{1}{d}[j_{\rm ext}-j_c\sin(\gamma_1)]\ ,\\ j_N'&=\frac{1}{d}[j_c\sin(\gamma_N)-j_{\rm ext}]\ .\end{aligned} \tag{7}$$

If a transport current is applied only along the c direction, this set of differential equations is completed by the boundary conditions

$$j_n(x=0)=j_n(x=b)=0\ .$$

Taking the derivative of (6) and using Maxwell's equation $\nabla\times\mathbf{H}=\mathbf{j}$ yields

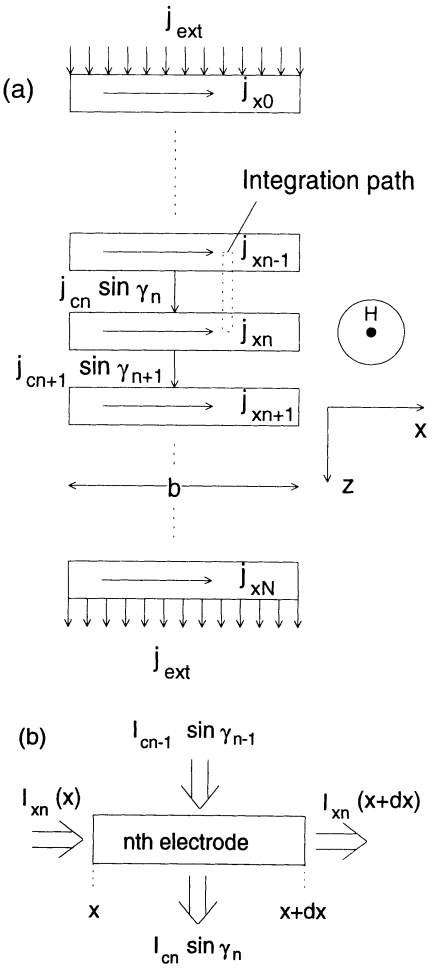

FIG. 2. (a) Stack of N Josephson junctions in a magnetic field parallel to the electrodes. Their thickness is assumed to be much smaller than the field penetration depth. (b) Schematic view of the currents passing a volume element of a thin electrode of a Josephson stack in the presene of a magnetic field and a bias current.

$$\gamma_n''=\frac{1}{\lambda_c^2}\sin(\gamma_n)+\frac{1}{\lambda_j^2}[2\sin(\gamma_n)-\sin(\gamma_{n-1})-\sin(\gamma_{n+1})]\ ,$$
$$\lambda_c=\left[\frac{\Phi_0}{2\pi\mu_0(t+d)j_c}\right]^{1/2}\ , \tag{8}$$
$$\lambda_j=\left[\frac{\Phi_0 d}{2\pi\mu_0\lambda_{ab}^2 j_c}\right]^{1/2}=\frac{\lambda_c}{\lambda_{ab}}\sqrt{(t+d)d}\ .$$

The same equation can be obtained from a rigorous treatment of the Lawrence-Doniach free energy.[54] The first term on the right-hand side is well known from the thick electrode limit where the factor $(t+d)$ is replaced by $(2\lambda_{ab}+t)$. It represents the self-fields due to the Josephson currents and is important if the junction length b is larger than λ_c. The second term, which is small in the case of thick electrodes, is due to the kinetic momentum of the supercurrents flowing along the electrodes. It obviously couples adjacent junctions. if the phaseses γ_n are not too different, this term is small. If, additionally, $\gamma_n \ll 1$, Eq. (8) reduces to

$$\gamma_n''=\frac{1}{\lambda_c^2}\gamma_n\ . \tag{9}$$

In this sense, λ_c can be defined as the magnetic penetration length with screening currents along the c direction.

For j_c between 100 and 7000 A/cm^2, as measured for BSCCO and PBSCCO, λ_c ranges between 30 and 400 μm, which is consistent with direct measurements of λ_c (Refs. 55 and 56) and also with γ values obtained from torque measurements.[30] For γ values between 200 and 1000, λ_j ranges between 0.14 and 0.7 μm.

If a and b are small compared to λ_c and λ_j, self-field and kinetic contributions can be neglected. Integration of (6) then leads to the well-known Fraunhofer pattern for the field dependence of the critical current,

$$I_c(H)=I_c(0)\left|\frac{\sin x}{x}\right|\ ,$$
$$x=\pi\frac{H}{H_0}\ ,\quad H_0=\frac{\Phi_0}{\mu_0 b(t+d)}\ . \tag{10}$$

This formula is similar to the thick electrode limit, where only the factor $(t+d)$ has to be replaced by $(2\lambda_{ab}+t)$. Taking $(t+d)=15$ Å and $b=1$ μm yields 1.3 T for the first zero of $I_c(H)$ at $H=H_0$.

Using the above considerations, we can now discuss the different types of measurements necessary to prove or disprove our model. Ideally, we would have to use single crystals with *ab* dimensions smaller than λ_j in order to be within the short junction limit and thus avoid complications due to the formation of Josephson vortices. Clearly, it is practically impossible to handle single crystals with *ab* dimensions much less than 1 μm. For the experiments we used single crystals with *ab* dimensions between 20 and 100 μm; i.e., we work in an intermediate region with $\lambda_j < a,b < \lambda_c$, where self-field effects are small but where currents flowing in the *ab* direction may strongly influence our results. However, in magnetic fields which are small compared to H_0, there is no reason to assume the presence of large *ab* currents, if the transport current flows strictly in the c direction. In the case of small *ab* currents, the second term on the right-hand side in Eqs. (6) and (8) is small, allowing us to work more or less within the short junction $(a,b \ll \lambda_c)$ limit. If, on the other hand, the *ab* currents are large (e.g., at $H=H_0$), Josephson vortices must form, which influence the current flow within the crystals.

The first evidence for Josephson coupling can be found from the shape of the *I-V characteristics*, with current flow in the c direction. As discussed above, we expect highly hysteretic curves if the intrinsic Josephson junctions are of the SIS type. Moreover, between the critical current I_c and the return current I_r, where the junctions return to zero voltage, each junction can be either in the resistive or in the superconducting state. Therefore the *I-V* characteristics should exhibit a large number of branches differing by the number of junctions in the resistive state. Such characteristics have been observed in Nb/Al-AlO$_x$/Nb multilayers.[43,57,58] If the junctions are of the SNS type, the *I-V* characteristics may be nonhysteretic. In this case the curvature d^2V/dI^2 must be positive in contrast to the negative curvature of flux-flow-type characteristics.

SIS and SNS-type junctions can be further distinguished by the *temperature dependence of the critical current*, $I_c(T)$. For SIS junctions the Ambegaokar-Baratoff relation (3) holds; i.e., $I_c(T)$ increases linearly near T_c and stays almost constant at low temperatures. In contrast, $I_c(T)$ of SNS junctions is parabolic at high temperatures and does not or only weakly saturates at low temperatures.[59,60]

As discussed above, special care must be taken in discussing the *magnetic-field dependence of the critical current*, $I_c(H)$. If we neglect complications due to *ab* currents, we would expect zeros of the Fraunhofer pattern at multiples of $H_0=450$ Oe for our typical crystal widths of 30 μm. Even then, however, small misalignments of the sample will lead to the formation of Abrikosov vortices penetrating the electrodes due to the large field scales required. These vortices will cause local variations of the critical current density in the c direction[61,62] and therefore strongly influence the Fraunhofer pattern. Nevertheless, the aim is to find modulations on a scale H_0 and to investigate their dependence on the crystal width b. If H_0 and b are known, the effective junction thickness can be inferred. Obtaining the expected value will be an important confirmation for the intrinsic Josephson effect and will rule out spurious effects.

The two final and most important tests of intrinsic Josephson coupling investigate the *ac Josephson effect*.

If a voltage V_n drops across the nth junction, the Josephson current will oscillate at a frequency

$$f_n=\frac{2e}{h}V_n\ . \tag{11}$$

The total voltage across the crystal is $V=\sum_{n=1}^{N}V_n$. If all

voltages V_n are equal, the Josephson currents of all junctions will oscillate at the same frequency and the total voltage is given by $V=NV_n$. Then the Josephson frequency-voltage relation is

$$f=\frac{2e}{h}\frac{V}{N} . \tag{12}$$

Even if the junction parameters are not completely identical, interactions between the junctions can lead to mutual phase locking and consequently to equal voltages.[63] Such interactions may be given by currents flowing in the *ab* direction (as discussed above), quasiparticles penetrating several electrodes, suppression of the amplitude of the order parameter within the electrodes, which couples adjacent junctions, or electromagnetic radiation. In Ref. 63 these mechanisms are discussed in detail.

Equation (12) can be examined in two ways. First, in an external microwave field, *Shapiro steps* will appear at voltages

$$V_k=\frac{h}{2e}kNf , \quad k=0,1,2,\ldots . \tag{13}$$

Shapiro steps of this kind have been found in quadratic[64] and linear[65] arrays of Josephson junctions. This kind of measurement requires a stable phase lock between the external microwave field and the Josephson currents as well as a mutual phase lock. For underdamped ($\beta_c>1$) junctions, this can either be achieved for frequencies well above the plasma frequencies or for very large microwave power.[45]

ac Josephson currents can be investigated in an easier, though technically more sophisticated way by direct detection of *microwave emission*. Radiation can be detected even without a stable phase lock. According to (12), at a fixed frequency, a maximum of the emitted power should occur at $V=N(h/2e)f$. Equation (12) can further be examined at different frequencies, revealing an independent determination of N. In the ideal situation, where all pairs of CuO_2 double planes are working Josephson contacts, N should equal the crystal thickness divided by 15 Å.

To summarize, the most effective means of identifying intrinsic Josephson junctions and distinguishing them from spurious effects such as cracks in the crystal is to infer the effective junction thickness from $I_c(H)$ measurements, to count the number of junctions from microwave emission experiments, and, in order to be sure that the detected power is due to Josephson radiation, to verify the Josephson frequency-voltage relation.

III. SAMPLE CHARACTERIZATION

$Bi_2Sr_2CaCu_2O_{8+x}$ (BSCCO) single crystals were grown from a stoichiometric mixture of the oxides and carbonates, heated up to 980 °C using Al_2O_3 or ZrO_2 crucibles and then cooled down to 800 °C at a rate of 1 °C/h. Composition and homogeneity of the crystals were checked by standard microprobe and x-ray analysis. Single crystals of the composition $(Bi_{1-y}Pb_y)_2Sr_2Cu_2O_{8+x}$ (PBSCCO), will lead contents y up to 20% have been grown by Regi *et al.*[66] $Tl_2Ba_2Ca_2Cu_3O_{10}$ (TBCCO) single crystals have been grown from a nonstoichiometric mixture of Tl_2O_3, $BaCuO_2$, CuO, and CaO powder by Winzer *et al.*[67] $YBa_2Cu_3O_7$ (YBCO) single crystals have been grown by Schönmann, Seebacher, and Andres.[68] Also, *a*-axis oriented YBCO films have been prepared by Baudenbacher,[69] by Hirata, and Kinder by thermal coevaporation at low substrate temperatures. The orientation was controlled by reflection high-energy electron diffraction (RHEED). For the transport measurements, thin (10×10 μm^2) bridges were patterned. The film thickness ranged between 1000 and 1500 Å. Preparation techniques of the PBSCCO, TBCCO, and YBCO single crystals are discussed in detail in Refs. 66–68.

The single crystals were cleaved in order to obtain small platelets with their largest dimensions in the *ab* direction. For *c*-axis transport experiments, gold layers were evaporated on both sample faces, followed by an anneal in Ar or O_2. The sample dimensions in the *ab* direction ranged between 20 and 100 μm, crystal thicknesses between 1 and 6 μm. The critical temperatures of the BSCCO single crystals, measured resistively, varied between 80 K for oxygen-annealed samples and 90 K for Ar anneal. The transition widths ΔT_c ranged between 0.5 and 3 K. The T_c of the PBSCCO crystals ranged between 55 and 92 K, depending on lead content and annealing condition. The ΔT_c was similar to that of the BSCCO crystals. The T_c of TBCCO was 118 K, $\Delta T_c=4$ K. The T_c of the YBCO films and single crystals was varied by oxygen anneal and ranged between 40 and 87 K.

The *c*-axis rsistivity ρ_c of the BSCCO and PBSCCO samples varied drastically as a function of oxygen and lead content (Fig. 3). Ar-annealed BSCCO crystals had a

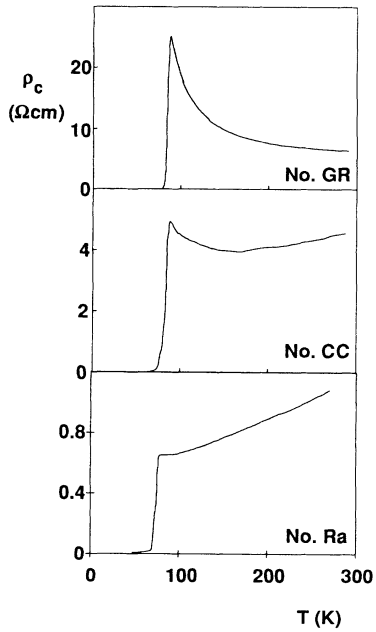

FIG. 3. Temperature dependence of the *c*-axis resistivity. Top: BSCCO, Ar anneal (12 h, 600°C), $T_c=86$ K; middle: BSCCO, O_2 anneal (36 h, 400°C), $T_c=83$ K; bottom: PBSCCO, $y=0.2$, O_2 anneal (10 h, 550°C), $T_c=76$ K. Contact resistivities are not subtracted.

TABLE I. Annealing conditions, sample dimensions, critical temperatures, critical current densities, and c-axis resistivities of the discussed samples.

Sample No.	Material	Annealing condition	Sample dimensions [μm^3]	T_c (ΔT_c) [K]	j_c (4.2 K) [A/cm^2]	$\rho_c(T_c)$ [Ω cm]
GR	BSCCO	12 h, 600 °C Ar	30×40×3	86 (4)	150	26
Ig	BSCCO	12 h, 600 °C Ar	90×100×3.5	87 (3)	150	28
Ld	BSCCO	12 h, 600 °C Ar	30×35×2.5	85 (3)		25
Id	BSCCO	12 h, 600 °C Ar	50×60×3	85 (2)	150	21
bur	BSCCO	10 h, 550 °C Ar	50×60×3.3	86 (3)	110	17
Rm	BSCCO	10 h, 550 °C Ar	45×60×2	86 (2.5)	140	17
sol	BSCCO	20 h, 550 °C Ar	60×70×3	85 (1.5)	100	20
Sh	BSCCO	163 h, 650 °C O_2	63×63×3	86 (4)	490	12
CM	BSCCO	20 h, 500 °C O_2	45×45×3	85 (3)	1050	4.3
Ph	BSCCO	170 h, 450 °C O_2	60×70×5	82 (3)	760	5.0
CC	BSCCO	36 h, 400 °C O_2	85×90×2.5	83 (3)	350	5.1
Ra	PBSCCO	10 h, 550 °C O_2	54×54×1.2	76 (2)	7200	0.7
Tlla	TBCCO	as grown	50×60×6	118 (2)	150	13

negative temperature coefficient between 300 K and T_c. At room temperature ρ_c was typically 6–8 Ω cm. Near T_c, values up to 70 Ω cm were observed. Upon oxygen anneal, ρ_c of the BSCCO samples became more metallic, but still had a slight upturn near T_c. Here ρ_c was typically 6 Ω cm for these samples. Because of the small crystal dimensions, we have not been able to measure the changes in the oxygen content x directly. However, from the measured T_c shifts and published T_c-vs-x data,[70] we estimate $\Delta x \approx 0.05$.

Lead substitution had similar consequences for ρ_c. Increasing the lead content changed the temperature coefficient of ρ_c from purely negative to a more metallic behavior.[66] These crystals were even more sensitive to annealing conditions. For samples with $y=0.2$ and oxygen anneal, purely positive temperature coefficients were obtained. For these samples, ρ_c at room temperature was below 1 Ω cm and T_c decreased to 76 K.

Critical current densities in the c direction, determined from I-V characteristics were typically 150 A/cm^2 at $T=4.2$ K for BSCCO single crystals annealed in Ar. Oxygen anneal as well as lead substitution led to an increase of j_c, reaching values up to 1.5 kA/cm^2 for oxygen-annealed BSCCO and 7 kA/cm^2 for oxygen-annealed PBSCCO with $y=0.2$. The critical current densities of the TBCCO single crystals were typically 200 A/cm^2.

Annealing conditions, sample dimensions, critical temperatures, transition widths, and c-axis resistivities of the samples discussed in this paper are listed in Table I.

The BSCCO single crystals used for c-axis transport experiments have also been investigated by angle-resolved torque magnetometry,[30,71] Raman spectroscopy,[72–74] muon spin relaxation (μSR),[75] electron-energy-loss spectroscopy (EELS),[76] and far infrared (FIR) spectroscopy.[77] These experiments also show strong variations of the crystal properties as a function of the oxygen content.

IV. MEASURING TECHNIQUES

To perform the c-axis transport measurements, a two-terminal technique was used. The crystals were mounted between two contact rods as shown in Fig. 4. The contact resistivity of the samples ranged between 10^{-6} and 10^{-4} Ω cm^2, which yields ratios of $R_{\text{contact}}/R_{\text{crystal}}$ of less than 0.05 for our typical crystal dimensions. In all figures shown below, the contact resistance is subtracted. Low-pass filters mounted in each current and voltage lead were used to shield external noise. For the magnetic-field measurements, the crystals were oriented by a two-axis goniometer. The misalignment of the ab planes relative to the external field direction was less than 0.5°. For the microwave absorption experiments (2–12 GHz, 20 dBm

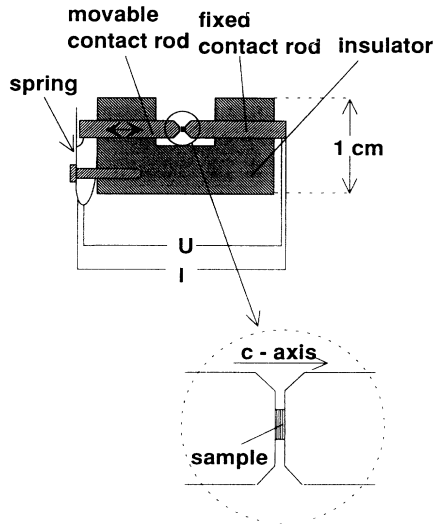

FIG. 4. Schematic view of the sample holder.

maximum output power), either Cu cavities or stripline configurations were used or the ac currents were coupled directly into the crystals using semirigid coaxial cables.

For the microwave emission experiments, the crystals were mounted inside a horn antenna at the end of an X-band waveguide. The signal was preamplified and mixed down with local oscillators at 10 GHz. The output voltage was either monitored at fixed detector frequency as a function of the voltage across the crystal or the spectral distribution was analyzed at a fixed voltage. The noise level of the system was -110 dBm at a bandwidth of 3 MHz. A similar setup has been used for the K-band measurements at 24.2 GHz. The noise figure of the downconverter was approximately 4.5 dB. For a comparable detection sensitivity, the bandwidth had to be increased to about 100 MHz.

In all cases current flow strictly along the c-axis had to be assured in order to avoid motion of Abrikosov vortices. We emphasize that, according to the discussion of Eqs. (6)–(10), current flow in the ab direction will additionally lead to the formation of Josephson vortices even in zero magnetic field, if the crystal dimensions are larger than λ_j (≈ 1 μm). This might explain the negative results of Tsai and Fujita, who performed transport measurements on BSCCO thin films using a geometry similar to the in-line geometry of long Josephson junctions.[78]

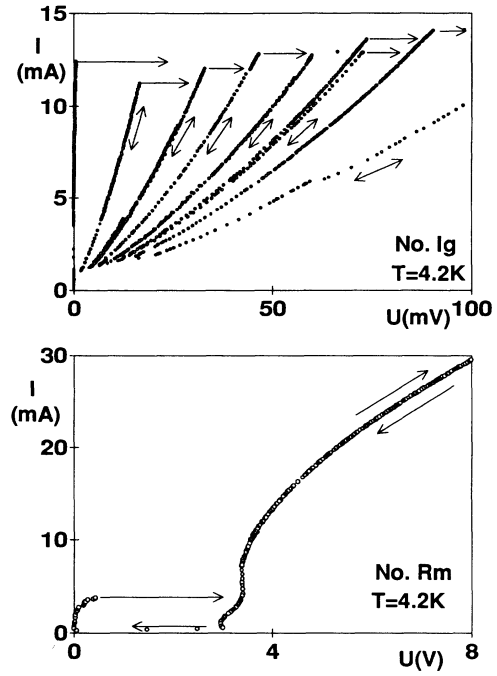

FIG. 5. I-V characteristics of Ar-annealed BSCCO crystals at different voltage scales. The multiple branches shown in the upper figure have not been traced out in the lower figure. The annealing conditions of the samples are 12 h, 600 °C (No. Ig) and 10 h, 550 °C (No. Rm). Contact resistances have been subtracted. Details of the I-V characteristics are described in the text.

V. RESULTS AND DISCUSSION

A. BSCCO and PBSCCO

1. *I-V characteristics*

Typical I-V characteristics of Ar-annealed BSCCO crystals at $T=4.2$ K are shown in Fig. 5. Increasing the bias current beyond I_c leads to several finite voltage jumps. If then the current is decreased, the voltage first changes continuously until it jumps back to a lower value and can be increased continuously again (arrows in Fig. 5, upper part). Ramping the current up and down repeatedly yields a large number of discrete branches of the I-V characteristics at successively higher voltages. We note that most of the branches are equally spaced, whereas some of them are lying close together. At bias currents well above I_c, the I-V characteristic becomes single valued and resembles I-V characteristics of standard SIS Josephson junctions (Fig. 5, lower part). At higher temperatures the hystereses decrease and disappear near T_c.

In the following we want to discuss the essential features of the I-V characteristics in order to show that all observations are fully consistent with a model of stacked SIS Josephson junctions.

a. Hysteresis and multiple branching. As discussed in Sec. II, from a preestimate of the junction parameters we expect the junctions to have highly hysteretic I-V characteristics. The almost equally spaced branches then differ by the number of (slightly different) junctions in the resistive state. Physically different groups, each having the same number of junctions, result in branches lying close together. From the I-V curves, we can infer characteristic voltages V_c of 12–15 mV. These values are close to the optimum value of 18 mV calculated from the zero-temperature Ambegaokar-Baratoff relation $V_c \approx I_c R = \pi/2e\Delta$, using $\Delta = 1.75kT_c$.

Alternatively, the observed branching might be interpreted in terms of zero-field steps known from long Josephson junctions.[79] In this case, however, the branches should rapidly tend to current steps which are due to resonant motion of vortex-antivortex pairs. In contrast to that, we always observe a finite resistance increasing with the branch number at fixed bias current. Therefore the above interpretation in terms of short underdamped Josephson junctions seems to be appropriate.

b. Gap features. At high voltages (i.e., with all junctions in the resistive state), the I-V curves exhibit a tunnelinglike quasiparticle curve with a "gap" value of 3.4 V. For the sample under discussion, the total number of Josephson junctions, calculated from the crystal thickness, is $N \approx 1000$, which results in an energy gap 2Δ of 3.4 mV per junction. This value is only 15% of the value expected from the BSC ratio and also too low with respect to the high characteristic voltages determined from the branches of the I-V curves at low voltages. However, such gap reductions have also been observed in Nb/Al-AlO_x/Nb multilayers.[43,57,58] Here the gap reduction as well as the appearance of a negative differential resistance at the gap voltage have been attributed both to Ohmic heating and to a gap suppression by quasiparticle injection.[80] Because of the extremely close-packed struc-

ture, both effects must clearly play an important role in BSCCO and might even be responsible for a very large gap suppression.

c. Critical current density. Finally, a consistency check can be made from a comparison of the critical current densities determined from the *I-V* characteristics and the *c*-axis penetration depth λ_c. According to Eq. (8), λ_c [μm]$=4100(j_c$ [A/cm^2]$)^{-1/2}$ For Ar-annealed BSCCO, j_c (4.2 K) = 150 A/cm^2 (cf. Table I) and thus $\lambda_c=335$ μm. This value is consistent with direct measurements which yield *c*-axis penetration depths between 100 and 500 μm, depending on the oxygen content of the crystals.[55,56] Furthermore, at 77 K we have determined an anisotropy ratio $\gamma=\lambda_c/\lambda_{ab}$ of approximately 900 and a penetration depth λ_{ab} (77 K)=7000 Å by angle-resolved torque measurements in Ar-annealed samples.[30] This yields $\lambda_c=630$ μm. With j_c (77 K) = 45 A/cm^2, Eq. (8) yields $\lambda_c=611$ μm in excellent agreement.

In the following we want to discuss the *I-V* characteristics of oxygen-annealed BSCCO and PBSCCO single crystals.

As shown in Fig. 4, the *c*-axis resistivity of these crystals is almost metallic in contrast to ρ_c of Ar-annealed samples. The critical current densities at $T=4.2$ K are much higher than in Ar-annealed crystals. They range from 300 to 1500 A/cm^2 for O_2-annealed BSCCO and reach values up to 7200 A/cm^2 for O_2-annealed PBSCCO. An enlarged coupling strength between the CuO_2 layers is further supported by torque measurements,[30] which show a decrease of the anisotropy factor γ down to values of $\gamma\approx150$. The possible occurrence of a decrease of anisotropy and strengthening of Josephson coupling by lead-substitution had been recently suggested on the basis of resistivity anisotropy measurements, and of considerations about the role of lead at the structural level (Ref. 66 and references therein). Nevertheless, the shape of the *I-V* curves is clearly Josephson-like. As an example, Fig. 6 shows an *I-V* characteristic of sample No. Ra (PBSCCO, $y=0.2$, annealed at 550 °C for 10 h) at $T=68$ K. The shape of the curve can be reproduced well by resistively shunted junction (RSJ) simulations with $\beta_C=2.1$. The characteristic voltage range typically between 0.5 and 1.5 mV. In contrast to the Ar-annealed crystals, even at high voltages no gap structures have been found, which indicates that either the junctions' normal resistance is mainly determined by parasitic shunts or the junction are of the SNS type. A decision between these possibilities can be found from the temperature dependence of I_c, as discussed below.

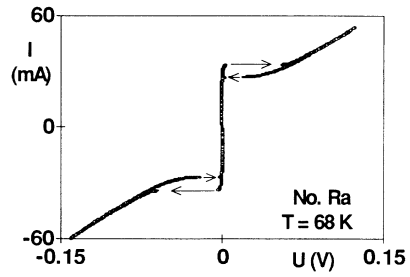

FIG. 6. *I-V* characteristic of sample no. Ra [$(Pb_{0.2}Bi_{0.8})_2Sr_2CaCu_2O_8$ (10 h, 550 °C O_2 anneal)] at $T=68$ K.

To conclude, although O_2 anneal and lead doping have obviously strongly altered the different junction parameters, the *c*-axis currents remain Josephson-like.

2. $I_c(T)$

The structure of the *I-V* characteristics indicates that at least Ar-annealed BSCCO crystals behave like stacks of SIS Josephson junctions. In this case, $I_c(T)$ should follow the Ambegaokar-Baratoff relation [Eq. (30)], which is clearly different from the $I_c(T)$ of SNS junctions. In the latter case, I_c tends to zero as $(1-T/T_c)^2$ near T_c and does not or only weakly saturates at low temperatures. In our experiments (Fig. 7), we find that $I_c(T)$ of oxygen-annealed samples can be fitted well by Eq. (3), if the usual BCS temperature dependence of the energy gap $\Delta(T)$ (Ref. 81) and a ratio $2\Delta(0)/k_BT_c=2.4$ are taken, which is slightly below the BCS ratio of 3.5. In contrast, $I_c(T)$ of Ar-annealed crystals is even above the SIS curve. First of all, the observed temperature dependence rules out SNS behavior both for the Ar- and O_2-annealed samples, because then $I_c(T)$ should stay well below the SIS curve. Second, the weak temperature dependence of the Ar-annealed samples may either be obtained by assuming nonequivalent electrodes (i.e., different order parameters in adjacent CuO_2 layers[50]) or by assuming a non-BCS temperature dependence of Δ. Whereas the first possibility does not seem to be reasonable, the second one is strongly supported by Raman measurements[74] determining the magnitude and temperature of the energy gap from the electronic spectra at low-energy transfers. For Raman and transport measurements, the same annealing conditions and crystals from the same batch have been used. A comparison of $\Delta(T)$ obtained from $I_c(T)$ by inversion of Eq. (3) as well as $\Delta(T)$ obtained from Raman data is shown in Fig. 8. The agreement between the two types of measurements is excellent. For oxygen-annealed crystals, Raman as well as our transport experiments obtained a BCS temperature of Δ, with $2\Delta(0)/k_BT_c=2.3$. For Ar-annealed crystals, both transport and Raman experiments yielded only weakly temperature-dependent

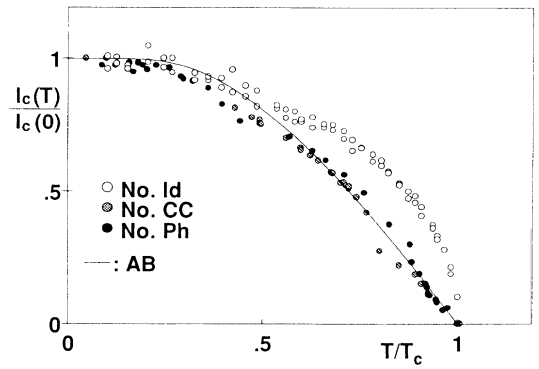

FIG. 7. $I_c(T)$ of an Ar-annealed (no. Id) and two O_2-annealed (no. Ph, no. CC) crystals. The solid line is the Ambegaokar-Baratoff relation for SIS junctions.

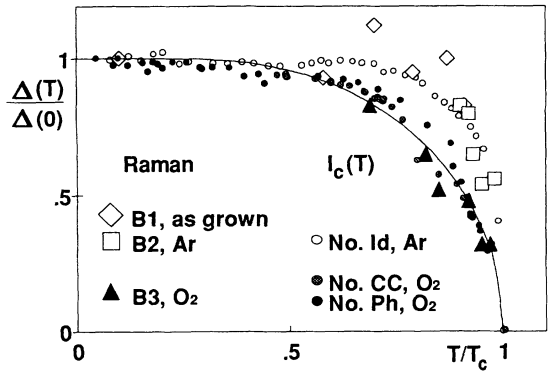

FIG. 8. Temperature dependence of the energy gap. Small symbols represent data obtained from $I_c(T)$ by numeric inversion of the Ambegaokar-Baratoff relation; large symbols represent Raman data. The solid line is the BSC temperature dependence.

gaps with $2\Delta(0)/k_BT_c=2.7$. So far, we do not have an explanation for the observed behavior of Δ. Nevertheless, the agreement between Raman and transport data further supports the picture of a stack of SIS Josephson junctions.

3. $I_c(H)$

One of the most crucial tests of our model is the magnetic-field dependence of the critical current, yielding the junction thickness as the most important information. As discussed in Sec. II, we cannot expect a pronounced Fraunhofer pattern due to the formation of Josephson and Abrikosov vortices. At least the latter complication can be minimized by a good alignment of the crystals (i.e., H parallel to the layers). In order to study the effect of misalignment, we first investigate $I_c(H)$ at different field orientations relative to the layers. The angle between **H** and the crystals' c axis is denoted ϑ.

For $\vartheta=0$, i.e., H perpendicular to the layers, we found a smooth field dependence of the critical current. It decreased to about 50% of its zero-field value in fields of typically 100–200 Oe (Fig. 9, solid triangles). The observed behavior is consistent with the field dependence of I_c, which has been calculated from Lawrence-Doniach theory by taking into account thermal fluctuations of Abrikosov vortices.[82]

We have determined the critical currents of the crystals as a function of ϑ at a fixed amplitude of the magnetic field. I_c peaks sharply for $\vartheta=90°$ (Fig. 10). If the field dependence of I_c would only be due to the field component perpendicular to the layers, $H_{\|c}=H\cos\vartheta$, a plot of the data of Fig. 10 vs $H_{\|c}$ would coincide with the direct $I_c(H)$ measurement with $\vartheta=0°$. Therefore a comparison between these plots directly shows the influence of the field component parallel to the layers. We have plotted the rescaled data of Fig. 10 as open circles in Fig. 9. The circles and triangles coincide at angles below 85°, thus showing that at a misalignment of more than 5° the I_c suppression is only due to the field component in the c direction.

The magnetic-field dependence of I_c for the "correct" field orientation ($\vartheta=90°$) is shown in Fig. 11(a) for

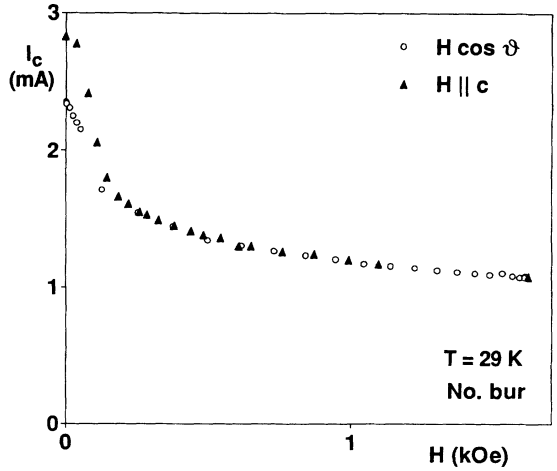

FIG. 9. $I_c(H)$ of sample no. bur (BSCCO, 10 h, 550°C, Ar) (triangles). The magnetic field was applied in the c direction. The circles are rescaled data from the angular dependence of I_c at a constant field of 1.6 kOe (see Fig. 10). At angles below 85°, $I_c(H)$ is determined only by the field component in the c direction.

$T=4.2$ K and 55 K. The misalignment of the crystal was smaller than 0.5°. We find clear modulations of the critical current on field scales $H_0=\Phi_0/\mu_0 b(t+d)$ (the "zeros" of the Fraunhofer pattern) at $T=55$ K, but only a flat curve at $T=4.2$ K, which is probably due to pinned vortices. Shallow modulations of I_c and a saturation of I_c at 80%–50% of its zero-field value were typical for all investigated samples.

We have found the same features in numerical calculations of $I_c(H)$ of a stack of five Josephson junctions using an extension of Eqs. (6)–(8), which includes electric fields and time-dependent terms [Fig. 11(b)]. In fields smaller than H_0, the simulations show a decrease of the critical currents of all junctions to about 60% of their zero-field

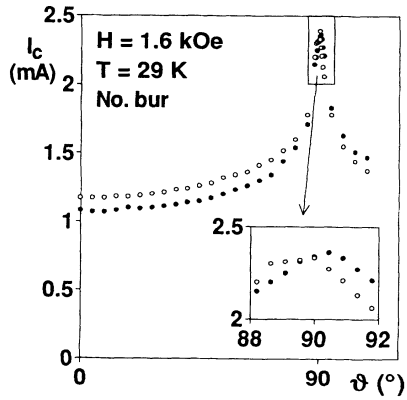

FIG. 10. I_c vs ϑ for sample no. bur (BSCCO, 10 h, 550°C, Ar). The sample was rotated from $\vartheta=0°$ (magnetic field in the c direction) to $\vartheta=90°$ (magnetic field in the ab direction). The magnetic field is $H=1.6$ kOe. The open (solid) circles correspond to positive (negative) values of the bias current. The crossover at $\vartheta=90°$ marks the reversal of the bias-current-induced self-field with respect to the external field direction.

values. In higher fields, I_c of the inner junction continues to decrease, whereas the critical currents of all other junctions stay almost constant up to $H \approx 2H_0$.[83] We note that the $I_c(H)$ plauteau can be obtained only from the above-mentioned full dynamic treatment. Because of computing time problems, we were not able to resolve modulations of $I_c(H)/I_c(H=0)$ smaller than 0.05 [Fig. 11(b)].

If the measured modulations of I_c can be interpreted as the "zeros" of the Fraunhofer pattern, they must scale as b^{-1} according to the above formula for H_0. We therefore investigated different crystals with ab dimensions between 20 and 100 μm. The result is shown in Fig. 12. The observed minima scale as b^{-1} and are consistent with a junction thickness of 15 Å. Therefore, also, the $I_c(H)$ test, though strongly influenced by the formation of vortices, clearly supports our model. Additionally, we note that quite similar $I_c(H)$ patterns have been observed in stacks of Nb/Al/AlO_x/Nb junctions,[43,57,58] which can be regarded as a model system for BSCCO.

4. *Microwave absorption*

The dc Josephson effects discussed above yielded mainly information on the properties of the single Josephson junctions, such as effective junction thickness or characteristic voltages. From the shape of the I-V characteristics and the temperature dependence of the critical current, we conclude that these junctions are of the SIS type. Through ac measurements we can study the properties of the stack of Josephson junctions as a whole.

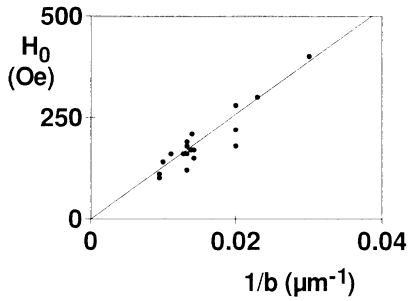

FIG. 12. First minimum in $I_c(H)$ vs crystal width b for different BSCCO single crystals; the solid line is given by Eq. (10) with an effective junction thickness of 15 Å.

According to Eq. (13), in a stack of N junctions we expect Shapiro steps to appear at voltages $V_k = (h/2e)kNf$, if the ac Josephson currents oscillate in phase. Phase locking of as many junctions as possible separates intrinsic Josephson effects from spurious ones, since it is unlikely that different random junctions can have almost identical properties. If all junctions can be synchronized, $N \approx 2000$ is expected. Of course, such an ideal case can hardly be expected. For the experiments, only frequencies below the plasma frequency and much smaller than the characteristic frequency were accessible, where phase lock in general is not stable.[45] We have found stable Shapiro steps in samples where some of the junctions exhibited small hystereses, probably as a result of parasitic shunts. The temperature and magnetic-field dependence of these junctions was identical to the results discussed above. An example with $N=17$ is discussed in Ref. 5. Frequency, as well as power dependence of the Shapiro steps, follows completely the well-known behavior of standard Josephson junctions. In some cases the Shapiro steps even cross the current axis (Fig. 13). Zero crossing

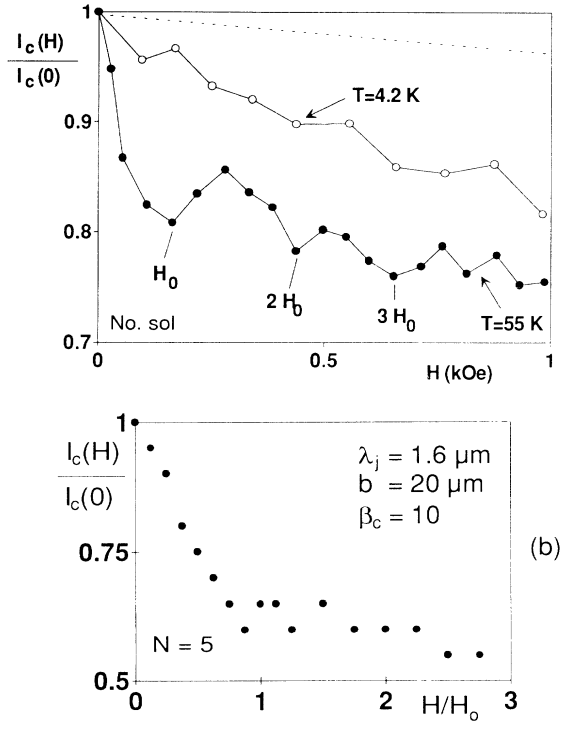

FIG. 11. (a) Magnetic-field dependence of I_c for sample no. sol (BSCCO, 20 h, 550°C, Ar) at $T=4.2$ and 55 K. The magnetic field was oriented parallel to the layers. The dashed line is an upper limit for the I_c suppression due to a misalignment of 0.7°. (b) Simulation of $I_c(H)$ of one of the outermost junctions in a stack of $N=5$ Josephson junctions. At $H=H_0=\Phi_0/\mu_0 b(t+d)$, the magnetic flux per junction equals one flux quantum. Note the numeric accuracy of $I_c(H)/I_c(H)$ of 0.05.

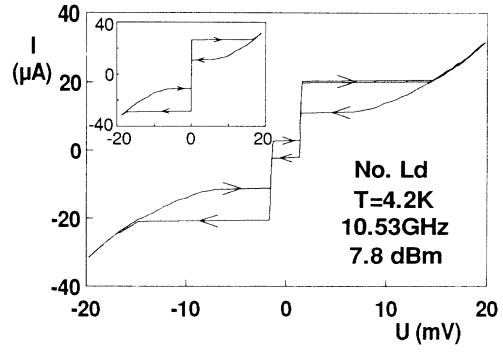

FIG. 13. Zero crossing steps, observed at a frequency of 10.5 GHz (no. Ld, BSCCO, 12 h, 600°C, Ar). Here 58 junctions have phase locked to the external frequency. The inset shows the I-V characteristic at zero power in the same units.

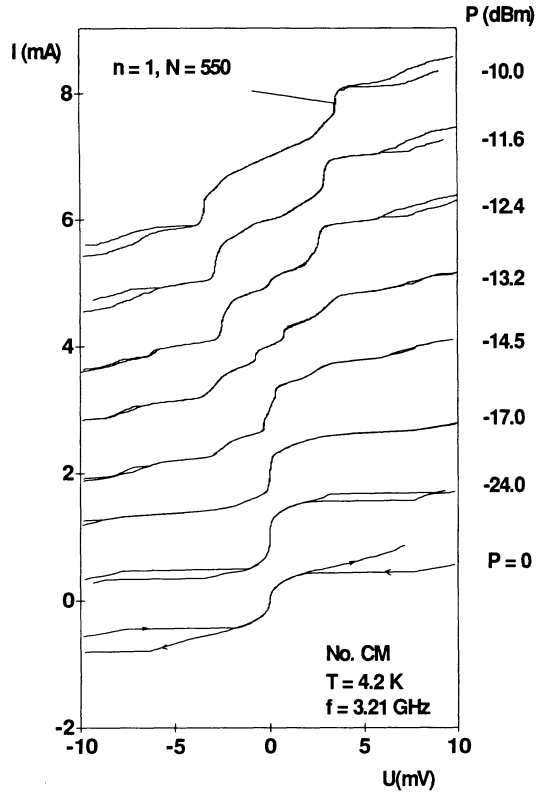

FIG. 14. *I-V* characteristics of sample no. CM at 3.2 GHz. The different graphs are offset vertically by 1 mA and are labeled with the microwave input power.

steps are known to appear if the applied frequency is on the order or above the plasma frequency, consistent with our preestimated values of 10 GHz for Ar-annealed crystals.

A more typical case is shown in Fig. 14. Also, here, clear constant-voltage steps can be seen. They are found at voltages in the mV range, indicating that several hundred junctions have phase locked. The step height exhibits the characteristic nonmonotonic power dependence. However, at increasing microwave power, the steps shift to higher voltages, which indicates that the number N of phase-locked junctions increases with increasing microwave power. Indeed, we have found the same behavior in the above-mentioned stacks of Nb/Al/AlO_x/Nb Josephson junctions.

5. *Microwave emission*

In order to introduce the basic principles of our measuring techniques, we first want to discuss the microwave emission observable in YBCO step edge junctions.[84]

According to the Josephson frequency-voltage relation, the ac Josephson current of a single Josephson junction oscillates at a frequency $f=(2e/h)V$, V being the voltage drop across the junction. The emitted microwave power is typically on the order of several picowatts. The most sensitive way to detect this radiation is to measure the emitted microwave power P at a fixed detector frequency as a function of the voltage drop across the junction. An example is shown in Fig. 15. The critical current at $T=63$ K is $I_c=100$ μA. The detector frequency is $f_D=12.45$ GHz. The emission peak occurs at $V_0=28.4$ μV, as expected from the Josephson frequency-voltage relation. The linewidth Δf of radiation can be calculated from the width ΔV of the peak $\Delta f=(2e/h)\Delta V$. In our case, Δf is as large as the detection frequency and one order of magnitude larger than expected for an ideal Josephson junction by taking only Nyquist noise into account ($\Delta f=40$ MHz per ohm junction resistance and kelvin[63]).

We now want to return to the intrinsic Josephson junctions. As shown above, the *I-V* characteristics of our crystals are highly hysteretic at low temperatures. Just above I_c there is a voltage drop of about 15 mV per junction for Ar-annealed BSCCO and typically 1 mV per junction for PBSCCO and O_2-annealed BSCCO. Lowering the bias current, this voltage can be decreased to 0.5 mV until the system returns to the superconducting state. Using the Josephson frequency voltage relation, we find that emission should occur at frequencies between 200 GHz and 7 THz, which is clearly out of our detection range. In order to obtain radiation at lower frequencies, we have to measure at temperatures close to T_c or use shunted single crystals.

Figure 16 shows an example of a PBSCCO single crystal at $T=4.2$ K, having a nonhysteretic *I-V* characteristic. The detection frequency is $f_D=24.2$ GHz. According to the discussion in Sec. II, we expect maximum emission at voltages $V_{\max}=N(h/2e)f_D$, which yields 50 μV per junction in this case. The maximum emission occurs at $V=9.2$ mV. Therefore we conclude that a stack of $N=190$ junctions contributes to the observed peak. Δf, as calculated from the width of the peak, is 2.5 GHz, one order of magnitude larger than expected for a perfect single junction.

In unshunted crystals we often find very sharp peaks at low temperatures.[38] Here the linewidth is as small as 8

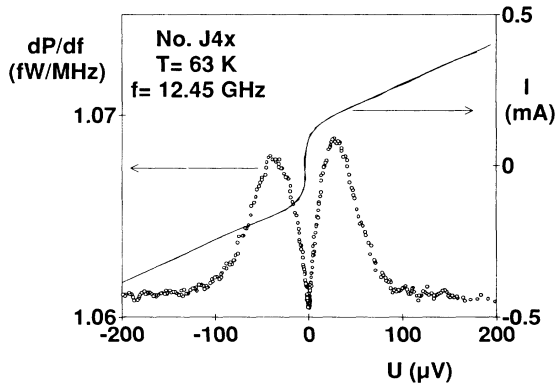

FIG. 15. *I-V* characteristic (right scale) and emitted microwave power (left scale) of YBCO step edge junction no. J4x at $T=63$ K. The detector frequency is 12.45 GHz. The maximum emission occurs at 25.8 μV as expected for a single Josephson junction.

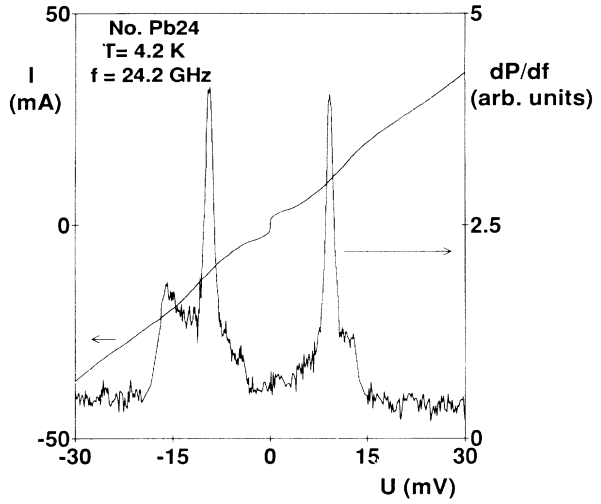

FIG. 16. *I-V* characteristic (left scale) and emitted microwave power (right scale) of sample no. Pb24 $[(Bi_{1.785}Pb_{0.125})_2Sr_2CaCu_2O_8]$ at $T=4.2$ K. The detector frequency is 24.2 GHz. The maximum emission occurring at 9.2 mV can be attributed to a packet of 190 junctions.

MHz. It is known[63] that the linewidth of radiation decreases like $1/N$, if N junctions are phase locked. Therefore we assume that these sharp peaks are due to groups of several tens of junctions radiating coherently.

In order to show that all junctions of the stack radiate, we now want to focus on temperatures close to T_c, where the *I-V* characteristics of all crystals are nonhysteretic. For a detection frequency of $f_D=11$ GHz and $N=2000$, we expect the maximum emission at $V=45.5$ mV. Figure 17 shows the emitted microwave power of No. Sh at two different frequencies. The emission peak shifts proportionally to the detector frequency. From the peak voltage, we deduce $N=1700$. The crystal thickness measured by scanning electron microscopy (SEM) is approximately 3 μm, which yields $N=2000$. Therefore we conclude that essentially all junctions within the crystal radiate. In order to confirm this result, we examined several

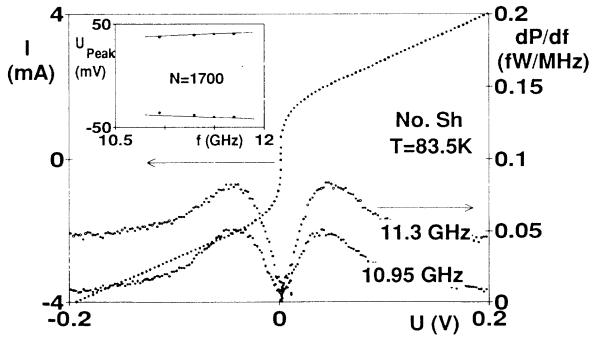

FIG. 17. *I-V* characteristic (left scale) and detected microwave power (right scale) of sample no. Sh (BSCCO, 163 h, 650 °C, O_2) at $T=83.5$ K. The detector frequencies were 10.95 and 11.3 GHz. Inset: Peak voltage vs detector frequency; the solid line is the Josephson voltage frequency relation for $N=1700$.

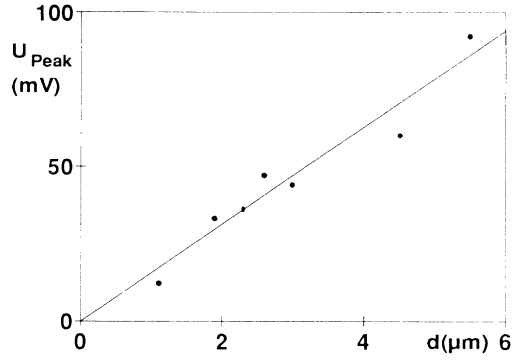

FIG. 18. Peak voltage of the emitted microwave power vs crystal thickness for different samples. The solid line is given by $U_{peak}=(h/2e)f$(crystal thickness)/(15 Å).

single crystals with thicknesses between 1 and 6 μm (corresponding to N between 670 and 4000). As shown in Fig. 18, the position of the maximum, U_{peak}, increases proportional to the crystal thickness. The slope of the solid line is given by $U_{peak}=h/2efN$, with N being simply the crystal thickness divided by 15 Å, and conforms nicely with our model.

B. TBCCO

In the 120-K compound TBCCO, CuO_2 triple layers are separated by BaO and TlO layers. The ansiotropy ratio γ determined from torque measurements is 900, similar to Ar-annealed BSCCO. The measured c-axis resistivities of the crystals between 10 and 15 Ω cm at room temperature and had a positive temperature coefficient. The structure of the *I-V* characteristics is essentially the same as for Ar-annealed BSCCO (Fig. 19). I_c vs T follows the Ambegaokar- Baratoff relation for SIS junctions (Fig. 20). We have also observed Shapiro steps in these crystals. Therefore it is evident that intrinsic Josephson effects also exist in TBCCO; i.e., this compound can also be described as a stack of SIS Josephson junctions.

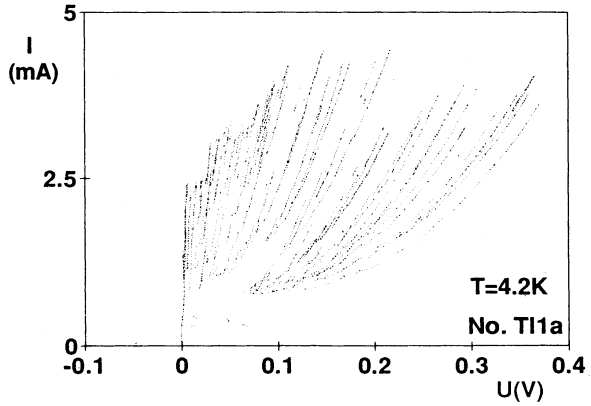

FIG. 19. *I-V* characteristic of sample no. Tl1a (TBCCO, as grown) at $T=4.2$ K.

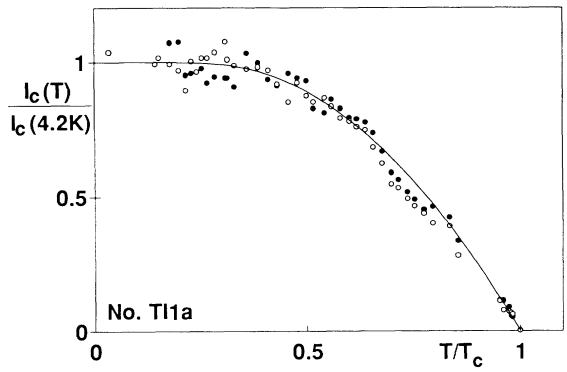

FIG. 20. Temperature dependence of the critical current of sample no. Tl1a (TBCCO, as grown). The solid line is the Ambegaokar-Baratoff relation for SIS junctions.

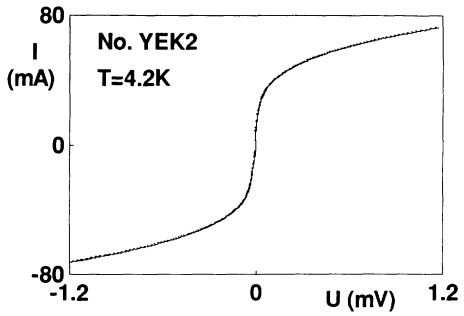

FIG. 21. *I-V* characteristic of YBCO single crystal No. YEK2 at $T=4.2$ K.

C. YBCO

YBCO is known to be much less anisotropic than the above compounds. For the fully oxygenated phase, with $T_c \approx 90$ K, the magnetic-field penetration depths are $\lambda_{ab} \approx 1400$ Å (Ref. 85) and $\lambda_c \approx 7000$ Å (Ref. 86) and thus $\gamma \approx 5$. For oxygen-deficient materials, λ_c increases up to 40 μm.[87] For the 90-K phase, the *c*-axis resistivities are less than 5 m Ω cm with a positive temperature coefficient. For the 60-K phase, ρ_c is about 50 m Ω cm at room temperature and has a negative temperature coefficient.[88] From H_{c2} measurements, *c*-axis Ginzburg-Landau coherence lengths of about 3 Å are calculated.[89]

Though YBCO is much less anisotropic than the above materials, ξ_c is smaller than the distance between the CuO_2 layers of 8.4 Å and therefore YBCO is still a candidate for a Josephson-coupled layered superconductor. However, the characteristic parameters are quite different from those of BSCCO and TBCCO: Equation (8) yields $\lambda_j \approx 32$ Å. Taking $\lambda_c = 7000$ Å, Eq. (8) yields a *c*-axis critical current density of more than 2×10^7 A/cm^2 at zero temperature.

For transport experiments we used single crystals of $40\times40\times5$ μm^3 in size and thin bridges patterned into *a*-axis-oriented thin films. Film thicknesses ranged between 1000 and 1500 Å; bridge dimensions were 10×10 μm^2. By oxygen anneal we varied T_c between 90 and 40 K. Typical results are shown in Figs. 21 and 22. In all cases we only observed flux-flow-like *I-V* characteristics. In microwave fields no evidence for Shapiro steps or other Josephson effects have been found. The result can be interpreted in two ways.

(a) YBCO is not Josephson coupled. Although the small *c*-axis coherence lengths indicate that in YBCO the order parameter still varies strongly in the direction perpendicular to the layers, this material may form a kind of S-S'-S structure, with weakly superconducting layers between the CuO_2 sheets.

(b) YBCO is still Josephson coupled, but we cannot identify Josephson effects. At least in the thin films these effects may be obscured by defects (e.g., dislocations, modulation of thickness, etc.). Second, all of our YBCO samples were much larger than λ_c and λ_j. Therefore we are clearly, in the large junction limit. In this case, vortices with dimensions of λ_{ab} in the *c* direction and λ_c along the layers will form parallel to the layers, creating the observed flux-flow behavior. Additionally, the intrinsic junctions may be of the SNS type, in contrast to BSCCO and TBCCO.

In recent experiments we found small microwave emission using *a*-axis-oriented films, which indicates that the second case is more probable. On the other hand, moving Abrikosov vortices will lead to microwave emission as well. Therefore we cannot distinguish between these possibilities at present. Additional investigations have to be done on this material.

VI. CONCLUSIONS

In summary, we have found clear evidence for intrinsic Josephson effects in $Bi_2Sr_2CaCu_2O_8$, $(Pb_yBi_{1-y})_2Sr_2CaCu_2O_8$, and $Tl_2Ba_2Ca_2Cu_3O_{10}$. In $Bi_2Sr_2CaCu_2O_8$, from the magnetic-field dependence of the *c*-axis critical current we have deduced an effective junction thickness of 15 Å, as expected for intrinsic Josephson junctions formed by a pair of CuO_2 double layers as the superconducting electrodes and the Bi_2O_3 and SrO layers as nonsuperconducting barriers. $I_c(H)$ flat-

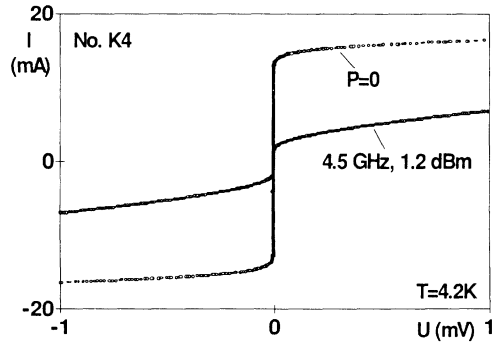

FIG. 22. *I-V* characteristics of *a*-axis-oriented YBCO film No. K4 at $T=4.2$ K without microwave irradiation and in a microwave field of 4.5 GHz. No Shapiro steps, only an I_c decrease was observed.

TABLE II. Classification of the results obtained in the different materials.

Material	T_c [K]	j_c (4.2 K) [A/cm^2]	Anisotropy $\gamma=\lambda_c/\lambda_{ab}$	V_c [mV]	Junction type
BSCCO, Ar anneal	86–90	100–200	1000	10–16	SIS
BSCCO, O_2 anneal	81–85	300–1500	> 150	0.5–1.5	SIS
PBSCCO, 20% Pb, O_2 anneal	65–75	7200		0.5–1	SIS
TBCCO, as grown	120	200	900	6–15	SIS
YBCO	40–92	no Josephson effects observed			

tens out rapidly if the flux per junction equals one flux quantum. At higher fields it stays approximately constant, exhibiting only shallow modulations at multiples of Φ/Φ_0. We note that this behavior is not due to sample imperfections, but can be explained by the vortex dynamics of a stack of Josephson junctions with ultrathin electrodes.

Microwave emission near T_c has demonstrated that the Josephson frequency-voltage relation holds, and most important, we have seen that, within experimental error bars, *all* intrinsic Josephson junctions (i.e., 2000 at a crystal thickness of 3 μm) radiate. From the temperature dependence of the critical current and from the shape of the *I-V* characteristics, we concluded that in all of these compounds the intrinsic junctions are of the SIS type. In BSCCO and PBSCCO, the junction parameters (j_c, V_c, β_c) can be varied strongly by oxygen and lead content (cf. Table II), which may be important for applications. Intrinsic Josephson effects have also been observed in the 120-K compound TBCCO, whereas the situation remains unclear in YBCO. Finally, we note that electrode thicknesses much less than the field penetration depth lead to length scales which differ strongly from standard Josephson junctions. Also, strong interactions between the junctions can be expected which require both experimental and theoretical investigations.

ACKNOWLEDGMENTS

We gratefully acknowledge valuable contributions by F. Steinmeyer, B. Avenhaus, C. Kreuzer, G. Kunkel, and P. Pospischil. We wish to thank H. Hagn, Physik Department E18, TU München, and Dr. W. Wersing, Siemens AG, München, for technological support. Part of this work was supported by the Bayerische Forschungsstiftung via the FORSUPRA consortium.

[1]W. Meissner and R. Ochsenfeld, Naturwissenschaften **21**, 787 (1933); R. Doll and M. Näbauer, Phys. Rev. Lett. **7**, 51 (1961); B. D. Josephson, Phys. Lett. **1**, 251 (1962).

[2]V. L. Ginzburg and D. A. Kirzhnits, in *High Temperature Superconductivity,* edited by J. L. Birman (Consultants Bureau, New York, 1982), pp. 213–240.

[3]A. I. Buzdin, B. U. Bujicic, and D. A. Kuptsov, Zh. Eksp. Teor. Fiz. **96**, 1094 (1989) [Sov. Phys. JETP **69**, 621 (1989)].

[4]D. I. Glazman and A. E. Koshelev, Zh. Eksp. Teor. Fiz. **97**, 1371 (1990) [Sov. Phys. JETP **70**, 774 (1990)].

[5]V. L. Pokrovskii and G. V. Uimin, Zh. Eksp. Teor. Fiz. **65**, 1691 (1974) [Sov. Phys. JETP **38**, 847 (1974)].

[6]V. M. Gvozdikov and E. Manninen, Fiz. Nizk. Temp. **9**, 1141 (1983) [Sov. J. Low Temp. Phys. **9**, 588 (1983)].

[7]I. O. Kulik and E. V. Minenko, Fiz. Nizk. Temp. **2**, 559 (1976) [Sov. J. Low Temp. Phys. **2**, 274 (1976)].

[8]L. N. Bulaevskii, Zh. Eksp. Teor. Fiz. **64**, 2241 (1973) [Sov. Phys. JETP **37**, 1133 (1973)].

[9]R. A. Klemm, A. Luther, and M. R. Beasley, Phys. Rev. B **12**, 877 (1975).

[10]Y. Seguchi, T. Tsuboi, and T. Suzuki, Physica B **165**, 1465 (1990).

[11]Y. Seguchi, T. Tsuboi, and T. Suzuki, Physica C **185**, 2035 (1991).

[12]D. Neerinck, K. Temst, C. Van Haesendonck, Y. Bruynseraede, A. Gilabert, and I. K. Schuller, Phys. Rev. B **43**, 8676 (1991).

[13]V. I. Dedyu, A. N. Lykov, and S. L. Prishchepa, Zh. Eksp. Teor. Fiz. **97**, 872 (1990) [Sov. Phys. JETP **70**, 488 (1990)].

[14]Q. S. Yang, C. M. Falco, and I. K. Schuller, Phys. Rev. B **27**, 3867 (1983).

[15]I. K. Schuller, Phys. Rev. Lett. **44**, 1597 (1980).

[16]I. Banerjee, Q. S. Yang, C. M. Falco, and I. K. Schuller, Solid State Commun. **41**, 805 (1982).

[17]I. Banerjee, Q. S. Yang, C. M. Falco, and I. K. Schuller, Phys. Rev. B **28**, 5037 (1983).

[18]I. Banerjee and I. K. Schuller, J. Low Temp. Phys. **54**, 501 (1984).

[19]T. W. Haywood and D. G. Ast, Phys, Rev. B **18**, 2225 (1978).

[20]G. Zheng, Y. Kitaoka, Y. Oda, K. Asayama, Y. Obi, H. Fujimori, and R. Aoki, J. Phys. Soc. Jpn. **60**, 599 (1991).

[21]L. N. Bulaevskii, Usp. Fiz. Nauk **116**, 449 (1975) [Sov. Phys. Usp. **18**, 514 (1975)].

[22]L. N. Bulaevskii, Adv. Phys. **37**, 443 (1988).

[23]T. Tsuzuki and T. Matsubara, Phys. Lett. **37A**, 13 (1971).

[24]E. I. Kats, Zh. Eksp. Teor. Fiz. **56**, 1675 (1969) [Sov. Phys. JETP **29**, 897 (1969)].

[25]S. A. Safran, Phys. Rev. Lett. **44**, 937 (1980).

[26]B. Y. Jin, J. B. Ketterson, E. J. McNiff, Jr., S. Foner, and I. K. Schuller, J. Low Temp. Phys. **69**, 39 (1987).
[27]Y. S. Kivshar and T. K. Soboleva, Phys. Rev. B **42**, 2655 (1990).
[28]W. E. Lawrence and S. Doniach, in *Proceedings of the 12th International Conference on Low Temperature Physics*, edited by E. Kanda (Academic Press of Japan, Kyoto, 1971), p. 361.
[29]M. J. Naughton, R. C. Yu, P. K. Davies, J. E. Fisher, R. V. Chamberlin, Z. Z. Wang, T. W. Jing, N. P. Ong, and P. M. Chaikin, Phys. Rev. B **38**, 9280 (1988).
[30]F. Steinmeyer, R. Kleiner, P. Müller, H. Müller, and K. Winzer (unpublished).
[31]I. Bozovic, J. N. Eckstein, M. E. Klausmeier-Brown, and G. F. Virshup, J. Supercond. **5**, 19 (1992).
[32]P. Schmitt, P. Kummeth, L. Schultz, and G. Saemann-Ischenko, Phys. Rev. Lett. **67**, 267 (1991).
[33]R. Marcon, E. Silva, R. Fastampa, and M. Giura, Phys. Rev. B **46**, 3612 (1992).
[34]A. V. Samoilov, A. A. Yurgens, and N. V. Zavaritsky, Phys. Rev. B **46**, 6643 (1992).
[35]N. V. Zavaritsky, A. V. Samoilov, and A. A. Yurgens, Pis'ma Zh. Eksp. Teor. Fiz. **55**, 133 (1992) [JETP Lett. **55**, 127 (1992)].
[36]R. Kleiner, F. Steinmeyer, G. Kunkel, and P. Müller, Physica C **185-189**, 2617 (1991).
[37]R. Kleiner, F. Steinmeyer, G. Kunkel, and P. Müller, Phys. Rev. Lett. **68**, 2394 (1992).
[38]B. Aigner, B. Avenhaus, R. Kleiner, C. Kreuzer, G. Kunkel, P. Pospischil, F. Steinmeyer, P. Müller, and K. Andres, IEEE Trans. Appl. Supercond. **3**, 2281 (1993).
[39]R. Kleiner, Ph.D. thesis, Technical University of Munich, 1992.
[40]B. Avenhaus, master thesis, Walther-Meissner-Institute, 1993.
[41]C. Kreuzer, master thesis, Walther-Meissner-Institute, 1993.
[42]G. Kunkel, master thesis, Walther-Meissner-Institute, 1992.
[43]P. Pospischil, master thesis, Walther-Meissner-Institute, 1992.
[44]C. Pegrum, Nature **358**, 193 (1992).
[45]R. L. Kautz and R. Monaco, J. Appl. Phys. **57**, 875 (1985).
[46]V. Ambegaokar and A. Baratoff, Phys. Rev. Lett. **11**, 104 (1963).
[47]J. Halbritter, Phys. Rev. B **48**, 9735 (1993).
[48]J. Halbritter, J. Supercond. **5**, 331 (1992).
[49]M. Däumling and G. V. Chandrasekhar, Phys. Rev. B **46**, 6422 (1992).
[50]A. Barone and G. Paterno, *Physics and Applications of the Josephson Effect* (Wiley, New York, 1982).
[51]M. Weihnacht, Phys. Status Solidi **32**, K169 (1969).
[52]S. Sakai, P. Bodin, and N. F. Pedersen, J. Appl. Phys. **73**, 2411 (1993).
[53]H. Amin, M. G. Blamire, and J. E. Evetts, IEEE Trans. Appl. Supercond. **3**, 2204 (1993).
[54]L. Bulaevskii and J. R. Clem, Phys. Rev. B **44**, 10 234 (1991).
[55]L. Forro, J. R. Cooper, B. Leontic, and B. Keszei, Europhys. Lett. **10**, 371 (1989).
[56]J. R. Cooper, L. Forro, and B. Keszei, Nature **343**, 444 (1990).
[57]I. P. Nevirkovets, H. Kohlstedt, G. Hallmans, and C. Heiden, Supercond. Sci. Technol. **6**, 146 (1993).
[58]H. Kohlstedt, G. Hallmans, I. P. Nevirkovets, D. Guggi, and C. Heiden, IEEE Trans. Appl. Supercond. **3**, 2197 (1993).
[59]P. G. deGennes, *Superconductivity of Metals and Alloys* (Benjamin, New York, 1966).
[60]K. K. Likharev, Rev. Mod. Phys. **51**, 101 (1979).
[61]M. V. Fistul, Pis'ma Zh. Eksp. Teor. Fiz. **3**, 193 (1990) [JETP Lett. **3**, 123 (1990)].
[62]S. L. Miller, K. R. Biagi, J. R. Clem, and D. K. Finnemore, Phys. Rev. B **31**, 2684 (1985).
[63]A. K. Jain, K. K. Likharev, J. E. Lukens, and J. E. Sauvageau, Phys. Rep. **109**, 309 (1984).
[64]S. P. Benz, M. S. Rzchowski, M. Tinkham, and C. L. Lobb, Phys. Rev. Lett. **64**, 693 (1990).
[65]D. W. Palmer and J. E. Mercereau, Phys. Lett. **61A**, 135 (1977).
[66]F. X. Regi, J. Schneck, H. Savary, C. Daguet, and F. Huet, IEEE Trans. Appl. Supercond. **3**, 1190 (1993).
[67]K. Winzer, G. Kumm, P. Maass, H. Thomas, E. Schwarzmann, A. Aghaie, and F. Ladenberger, Ann. Phys. (Leipzig) **1**, 479 (1992).
[68]K. Schönmann, B. Seebacher, and K. Andres, Physica B **165&166**, 1445 (1990).
[69]F. Baudenbacher, K. Hirata, and H. Kinder (unpublished).
[70]C. Allgeier, Ph.D. thesis, University of Munich, 1990.
[71]F. Steinmeyer, R. Kleiner, and P. Müller, Physica C **189**, 2381 (1991).
[72]T. Staufer, R. Hackl, and P. Müller, Solid State Commun. **75**, 975 (1990).
[73]T. Staufer, R. Hackl, and P. Müller, Solid State Commun. **79**, 409 (1991).
[74]T. Staufer, R. Nemetschek, R. Hackl, P. Müller, and H. Veith, Phys. Rev. Lett. **68**, 1069 (1992).
[75]H. Maletta (unpublished).
[76]N. Nücker, U. Eckern, J. Finck, and P. Müller, Phys. Rev. B **44**, 7155 (1991).
[77]A. Zibold, M. Dürrler, A. Gaymann, H. P. Geserich, N. Nücker, V. M. Burlatov, and P. Müller, Physica C **193**, 171 (1992).
[78]J. S. Tsai and J. Fujita (unpublished).
[79]T. A. Fulton and R. C. Dynes, Solid State Commun. **12**, 57 (1973).
[80]S. M. Faris, Physica **126B**, 165 (1984).
[81]B. Mühlschlegel, Z. Phys. **155**, 313 (1959).
[82]L. L. Daemen, L. N. Bulaevskii, M. P. Maley, and J. Y. Coulter, Phys. Rev. Lett. **70**, 1167 (1993).
[83]R. Kleiner, P. Pospischil, P. Müller, and H. Kohlstedt (unpublished).
[84]W. Reuter, M. Siegel, K. Hermann, J. Schubert, W. Zander, A. I. Braginski, and P. Müller, Appl. Phys. Lett. **62**, 2280 (1993).
[85]S. Sridhar, D. H. Wu, and W. Kennedy, Phys. Rev. Lett. **63**, 1873 (1989).
[86]S. Mitra, J. H. Cho, W. C. Lee, D. C. Johnston, and V. G. Kogan, Phys. Rev. B **40**, 2674 (1989).
[87]H. Veith, Ph.D. thesis, Technical University of Munich, 1992.
[88]T. Ito, H. Takagi, S. Ishibashi, T. Ido, and S. Uchida, Nature **350**, 596 (1991).
[89]U. Welp, W. K. Kwok, G. W. Crabtree, K. G. Vandervoort, and J. Z. Liu, Phys. Rev. Lett. **62**, 1908 (1989).

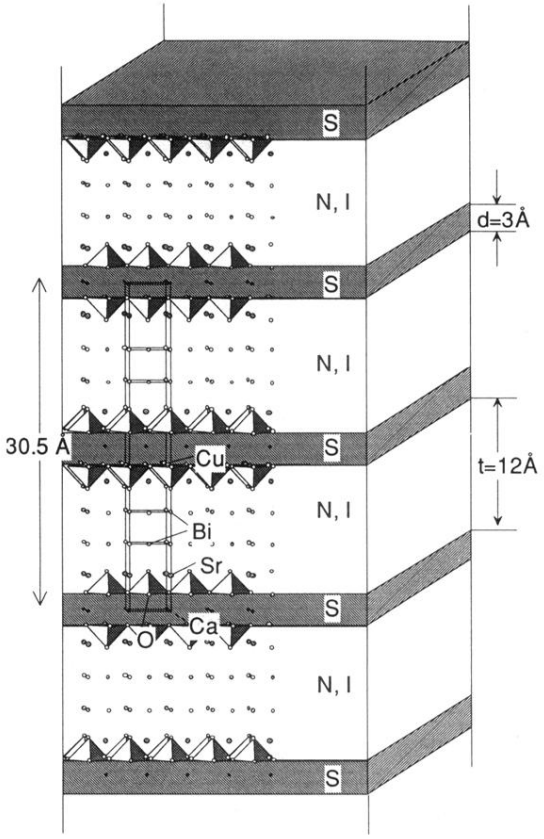

FIG. 1. Superposition of the BSCCO crystal structure and a stack of Josephson junctions, whose electrodes are formed by CuO_2 double layers.